Geophys. J. Int. (2007) **169,** 357–364 doi: 10.1111/j.1365-246X.2006.03307.x

Deformation between 1989 and 1997 at Piton de la Fournaise volcano retrieved from correlation of panchromatic airborne images

Marcello de Michele[1] and Pierre Briole[2]

[1] *Bureau de Recherches Géologiques et Miniéres, Orléans, France. E-mail: m.demichele@brgm.fr*
[2] *UMR CNRS* 7531, *Institut de Physique du Globe de Paris, Equipe de Géodésie et Gravimétrie, Paris, France*

Accepted 2006 November 20. Received 2006 November 19; in original form 2005 July 27

SUMMARY

We processed two panchromatic airborne images in the attempt to measure deformation on Piton de la Fournaise volcano between 1989 and 1997. Piton de la Fournaise erupted three times during 1989–1997 with fissures opening near Dolomieu summit crater. During this period no Synthetic Aperture Radar Interferometry data were available and only few geodetic points surveyed the summit crater. We therefore, apply for the first time the subpixel image-correlation technique on airborne images for monitoring ground deformation on Piton de la Fournaise volcano. Correlogram analysis reveals cumulative deformation in the summit area. We observe ESE spreading of the summit caused by the inflation–deflation cycle during 1989–1997. We calculated relative ground displacement along both sides of the main eruptive fissures, finding a maximum of 1.8 ($\pm$0.42) m opening. Direct comparison between deformation retrieved by correlation and available geodetic data at four locations shows qualitative agreement. We demonstrate the potential of subpixel image correlation technique, using panchromatic airborne images, for deformation monitoring on volcanoes. We also illustrate the capability of this technique for remote lava flow mapping.

Key words: deformation, image correlation, Piton de la Fournaise, volcanic activity.

1 INTRODUCTION

Piton de la Fournaise, La Reunion Island, France, is an active basaltic shield volcano (Fig. 1). Most of its recent effusive activity, including the 1990, 1991 and 1992 eruptions, is located within the Enclos Fouqué caldera. Eruptive fissures are mainly located near the central crater, Dolomieu. The fissure pattern on Piton de la Fournaise outlines two unstable rift zones trending NE and SE, respectively, where most eruptions and dyke intrusions occur, while most pre-eruptive swarm earthquakes occur under Dolomieu summit crater (Nercessian *et al.* 1995). Deformation and flank spreading is also localized in the summit area, being well correlated in time and location with eruptions (Briole *et al.* 1998). Several studies have shown that flank spreading on Piton de la Fournaise might result from both dyke intrusions and gravitational sliding towards low confinement areas (e.g. Lenat *et al.* 2001; Merle & Lenat 2003).

The year 1998 marked the end of 5 yr quiescence at Piton de la Fournaise volcano. While eruptions occurring from 1998 to the present have been studied by remote sensing techniques (e.g. Sigmundsson *et al.* 1999; Froger *et al.* 2004; Fukushima *et al.* 2005), the period 1989–1997 lacks similar data. Moreover, between 1989 and 1997 there are far fewer ground geodetic data than now, with GPS used increasingly since 1992 but especially since 1999 when more portable units became available. In this study, we focus on the period 1989–1997, in an attempt to measure ground displacement by an image correlation technique applied to panchromatic airborne images. Image correlation techniques represent a valuable complement to Differential Synthetic Aperture Radar Interferometry (DInSAR), in particular, near faults and fracture zones where large displacements result in a poorly coherent SAR signal. This technique has been successfully applied using both SAR amplitude images and satellite/airborne optical images in different fields of study. In particular, in seismo-tectonics (e.g. Michel & Avouac 1999; Van Puymbroeck *et al.* 2000; Michel & Avouac 2002; Dominguez *et al.* 2003; Binet & Bollinger 2005; Fialko *et al.* 2005; Kninger *et al.* 2006; Michel & Avouac 2006) in volcano deformation (Tobita *et al.* 2001) and in gravitational movement assessment (e.g. Delacourt *et al.* 2004; Berthier *et al.* 2005). Nevertheless, this is the first time that the correlation technique has been applied to panchromatic airborne images for quantifying volcano deformation.

2 ERUPTIVE ACTIVITY ON PITON DE LA FOURNAISE (1989–1997)

Three basaltic eruptions took place in the period 1989–1997 at Piton de la Fournaise volcano in 1990, in 1991 and in 1992 (Toutain *et al.* 1990, 1991, 1992a) (Fig. 2). These eruptions occurred in an unpopulated area and did not induce any threat to property.

The 1990 eruption began on January 18 from both the E interior of the Dolomieu crater and SE Dolomieu upper flank where it propagated S–SE for several hundreds of metres. During the dyke

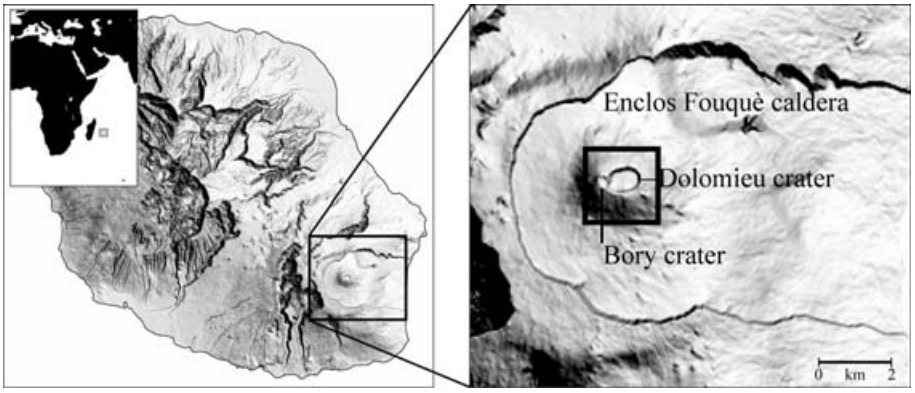

Figure 1. Study area. Piton de la Fournaise volcano, La Reunion Island, Indian Ocean. Black box in the right image represents the study area in Fig. 3.

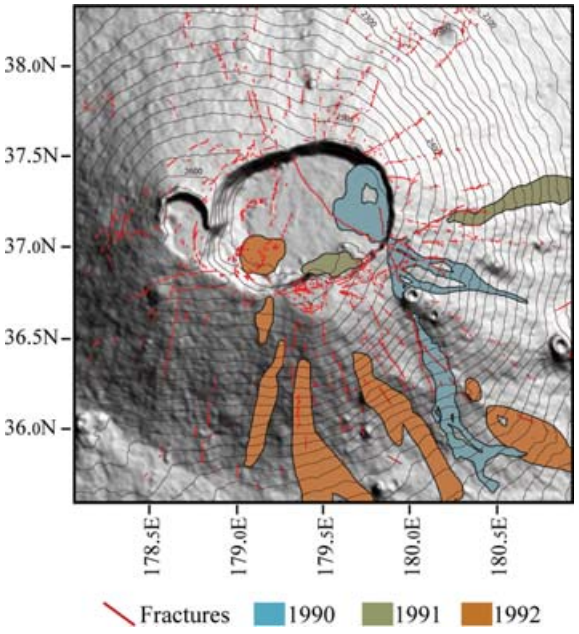

Figure 2. Map representing the 1990, 1991 and 1992 lava flows at Piton de la Fournaise after Toutain *et al.* (1990,1991,1992a). The lava flows have been plotted on the DEM. Red lines represent the main fractures within the study area. Units are in km, Gauss–Laborde map projection.

injection, tilt-metres recorded migration of the deformation centres in the same direction as the feeding fracture (Toutain *et al.* 1990).

The 1991 eruption started on July 19. Lava was emitted from two fissures along an eruptive fissure trending ENE. One fissure was localized inside Dolomieu crater, erupting some lava along its SE border. The other fissure was localized outside Dolomieu crater (Toutain *et al.* 1991).

The 1992 eruption began on August 27 from a fissure within the E–W Dolomieu crater area. The fissure propagated rapidly southward, crossing the rim. Four additional fissures opened SE of the first fissure. The seismic pattern suggested a small magma pocket fed the intrusion moving up towards Dolomieu (Toutain *et al.* 1992a). The tilt-metre pattern suggested general inflation of Dolomieu crater (Toutain *et al.* 1992b).

3 DATA

Two panchromatic airborne images have been used in this study (Fig. 3). Both the images have been acquired using wide-angle cameras during two Institut Géographique National (IGN) photogrammetric surveys. The first image was acquired during a 1989 survey (mission REU, 112, P) at 1:20.000 scale. The second image was acquired during a 1997 survey (mission REU, 119, P) at 1:30.000 scale. Both have been scanned at 1300 dpi (dots per inch) resolution, 8-bit pixel depth.

There are several reasons for selecting the aforementioned images. First, both images cover the summit volcanic area, which is the place where we knew deformation had been active in the period 1989–1997, with the deformation sometimes visible in the field (e.g. new eruptive fissures from decimetres to metres opening). Secondly, the base to height ratio (B/H) between the chosen images is the smallest among the entire set of available images**,**which minimizes the effect of topography on the offset measurements. Thirdly, the pixel size (0.5 m for 1989 images and 0.7 m for 1997 images) suits the requirement for fissure opening measurements using subpixel correlation analysis.

We used a five metre grid size Digital Elevation Model (DEM) as a geo-coded reference surface in the orthorectification process. The DEM covers a 25 km^2 area on top of Piton de la Fournaise. The DEM accuracy has been tested against over 10 000 kinematic differential GPS points (DGPS) (Trembley & Briole 2005). The standard deviation between the DEM and the DGPS profiles has been found to be 1.5 m with a maximal error of 3 m.

4 DATA PROCESSING AND ACCURACY ASSESSMENT

The image correlation technique relies on the statistical analysis of two sets of data (e.g. digital panchromatic imagery). This technique matches the 'before' image (1989) and the 'after' image (1997) at each point on a grid, analysing the degrees of local correlation at each step. Differences in the local instantaneous frequency of the images result in subpixel spatial differences in ground patterns (Crippen 1992). The results are an expression of both movements in the ground surface and image distortions. Sources of image distortions are very well discussed in Michel & Avouac (2006). Distortions mainly depend on the B/H, where B is the perpendicular distance between the two airplane positions and H is the altitude above the datum. The B/H controls the stereoscopic effect, and therefore, the degree of local differences in both scale and feature position between the two air-photos. Moreover, when correlating two images, the B/H determines the level of quality the DEM has to have, given that the higher the B/H the higher the apparent horizontal displacement that would be induced by an error in the DEM (Van Puymbroeck *et al.*

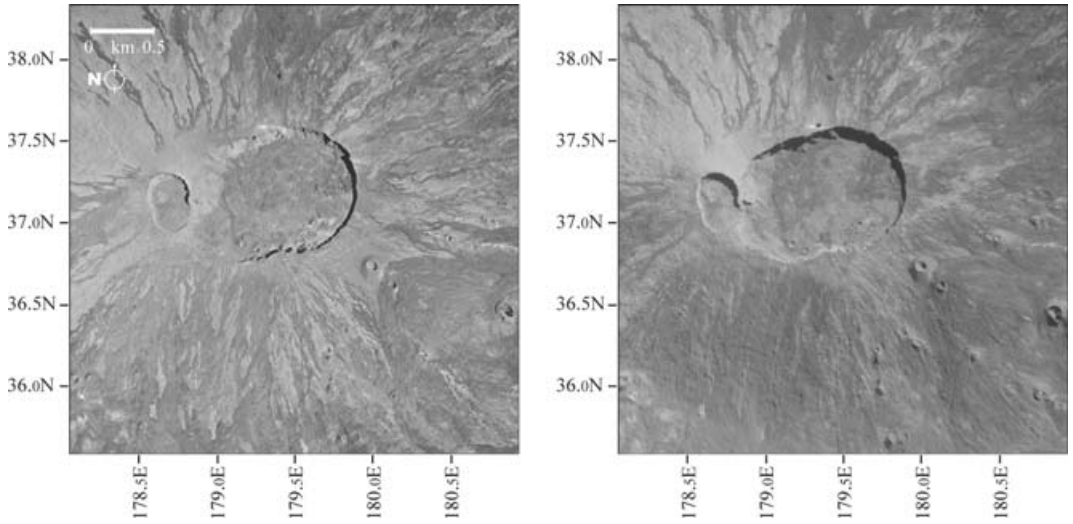

Figure 3. Piton de la Fournaise summit area. 1989 orthoimage (left), 1997 orthoimage (right). These are the images we have used in the correlation analysis. Notice the differences in solar illumination, and surface changes due to new lava flows. Units are in km, Gauss–Laborde map projection.

2000). In a hypothetical case where both the images have been acquired from exactly the same position ($B/H = 0$), one would not need to perform any ortho-rectification since there would not be any stereoscopic effect. In our case ($B/H \approx 0.25$), an error of 1.5 m in the DEM would create an apparent horizontal displacement of $\sim$0.3 m ($\sim$0.4 pixel). Since a finer DEM is not available, 0.3 m represents one significant limit in the accuracy of our measurements. Another source of distortion might come from the camera lens. This distortion is virtually zero at the centre of the scene and increase towards the edges. Our photos have been acquired by a metric camera so that the degree of distortion rate versus the lens radius is a known parameter that can be compensated during resampling.

The image correlation technique requires both the airborne images to be re-projected into the same geometry before calculating subpixel cross-correlation. Therefore, images are first projected into the DEM geometry (Orthorectification). In the orthorectification process we used both the metric camera parameters and 40 ground control points (GCPs). The viewing camera parameters have been provided by IGN while the GCPs have been retrieved from both the GPS network at Piton de La Fournaise and selected points on kinematic GPS profiles from Trembley & Briole (2005). Moreover, 20 tie points identified on both the images have been used to improve coregistration. Both the images have then been resampled to 0.7 m pixel size using a cubic convolution in order to preserve radiometric quality. Uncertainties on the viewing camera parameters are minimized in the process of orthorectification. However, a residual low wavelength error might bias the results. An empirical estimate of the cumulative effects of all unmodelled sources of errors could not be performed in this study due to the lack of quality data in non-deforming periods prior to 1989. Therefore, somehow our error assessment is underestimated. Michel & Avouac (2006) have shown that unmodelled errors other than the DEM uncertainty might account for another $\sim 1/3$ of the overall error. This yields a comparative estimate which we use to reassess the accuracy of our offset measurement to ± 0.42 m.

The correlation analysis has been performed by the use of MEDICIS software. MEDICIS allows subpixel offset measurements by means of a sliding NxM window (Centre National d'Etude Spatiales, 2000) with an accuracy of 1/10 pixel. The size of the sliding window is chosen according to local differences in the radiometry of the input images. Each pixel is a measure of the radiance and each digital number changes according to differences in either solar illumination or surface changes, mainly. Therefore, on the one hand, a small window would be too sensitive to noise (i.e. random radiometric changes). On the other hand, a large window would be less sensitive to non-uniform offsets. In this case study, a 31×31 pixel sliding window has been used. It yields independent measurements every 16 pixels (11.2 m). The local correlation coefficient (ρ) is calculated between the two images at each step of the grid. The local correlation coefficient is a normalized value that varies between 0 and 1. It gives an assessment of the radiometric differences between the images, and therefore, provides us with an estimate of the uncertainties on the measurements; that is, below a particular threshold the measurement is not reliable. In this study, we do not use offset values with $\rho \leq 0.4$. Radiometric changes typically reflect physical variations occurring on the ground between the acquisition of the two photos. Differences in solar illumination and random surface changes (like erosion phenomena or lava flows) result in poorly correlated pixels.

5 QUANTIFICATION OF DISPLACEMENT

Fig. 4 shows the results of correlation analysis between the 1989 and the 1997 images. Figs 4(a) and (b) represent the East and South offset, respectively. These data represent the cumulative ground displacement of the summit area of Piton de la Fournaise over an eight year period. They show that the summit area experienced ground deformation due to the inflation/deflation cycle triggered by dyke intrusions in 1990–1991–1992. Deformation is mainly localized southeast of Dolomieu crater where north–south oriented fissures opened during the eruptions. This sector is collapsing southeastward. In this sector of the volcano, our data show a spatially continuous displacement field, which we think is due not only to opening of new fissures but also to reactivation of ancient fractures. In fact, ground deformation is not only localized in the vicinity of each new eruptive fissure but also shows up with a clear coherent signal around ancient fractures that were not erupting during 1989–1997. We inferred the ancient fractures from direct observation of the orthoimages in 1989 and 1997 (plotted in white in Figs 4c and d).

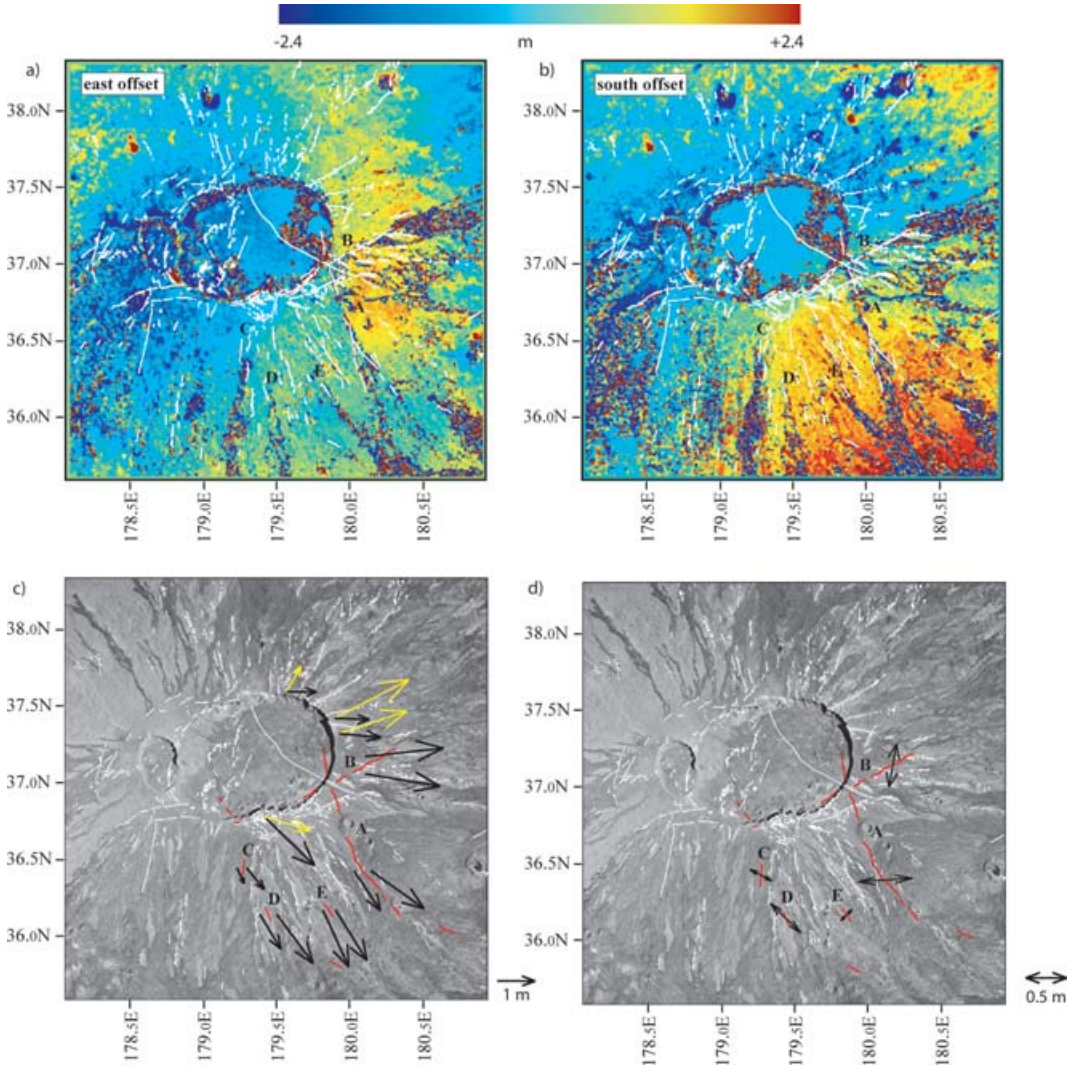

Figure 4. Correlation analysis results. Offsets between 1997 orthoimage and 1989 orthoimage have been calculated. (a) east offset, (b) south offset, (c), GPS velocity vectors, in yellow, compared with offset values, in black, along main eruptive fissures and at GPS locations and (d) averaged absolute fracture widening along main eruptive fissures. Noisy values in (a) and (b) correspond to poor correlation areas where large differences in radiometry exist between the two images (e.g. the 1990 lava flow, east of the Dolomieu crater interior). Differences in solar illumination also affect the quality of the correlation in the steeper areas. We superimposed the fracture map, in white, on the offset measurements (a) and (b). Areas with stronger deformation gradients correspond to the location of the 1990, 1991 and 1992 eruptive fissures. A spatial relationship between fractures and displacement offset is clear also for several pre-existing fractures, which are not directly related to the 1990, 1991 and 1992 dykes intrusions.

We suggest that, during the process of inflation, the ground begins to deform in areas of weak resistance (i.e. ancient fractures) while the new dyke is intruding and creating a new fissure. The few available geodetic measurements from Briole *et al.* (1998) (yellow vectors in Fig. 4c) show that magnitude and direction of the deformation inferred by field geodesy is comparatively consistent with displacement field inferred by correlation (Table 1). Differences can be partly explained by the fact that field geodesy displacements are calculated on a slightly different time period (1985–1992) and they represent point wise values. Correlation results quantify cumulative displacements across 1989–1997 and are characterized by spatially continuous analyses where each pixel embodies information about averaged displacement occurring within 21.7 m on the ground (31 × 31 pixel).

We think that long wavelength features in the offset field (lower than 1 km^{-1}) represent cumulative volcano inflation. Nevertheless, the uncertainty on aerial image offset measurements at this long wavelength is significantly higher due to unmodelled low frequency bias thus preventing precise quantitative long-wavelength deformation assessment.

Table 1. Comparison between North and East components of deformation vectors measured by geodetic surveys (N_g, E_g) and by offset (N_o, E_o) at points locations I, II, III and IV. Refer to figure 4(c), where point location I is the northernmost point followed by point II, III and IV clockwise. M_g and M_o represent vectors magnitude in metres.

	N_g	N_o	E_g	E_o	M_g	M_o
I	0.61	**0.01**	0.42	**0.59**	0.73	**0.77**
II	1.30	**−0.30**	1.88	**0.88**	2.20	**0.92**
III	0.83	**−0.33**	1.53	**0.94**	1.74	**0.99**
IV	−0.45	**−1.31**	1.21	**1.23**	1.29	**1.78**

We estimated the distribution of perpendicular and parallel relative motion across the 1990, 1991 and 1992 eruptive fissures

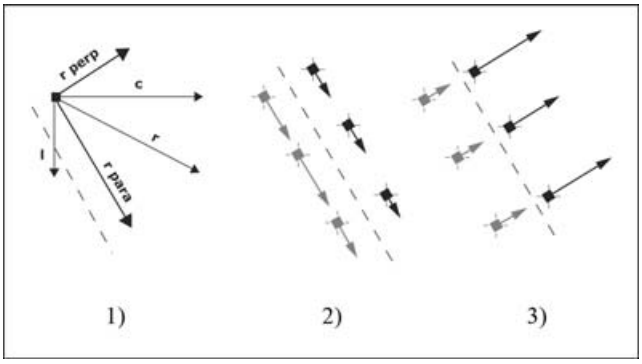

Figure 5. (a) Illustration of the method used to produce graphs in Figs 5(b) and 5(c). The offset perpendicular (*r* perp) and parallel (*r* para) component in respect to fissure direction (dashed line) is shown in (1). **l** and **c** represents the original offset lines and columns vectors at given geographic location. (2) and (3) represents the methodology that we used for offset measurements across eruptive fissures. 5(b) Estimation of the offset (parallel and perpendicular components) of the 1990 (A) and 1992 (C, D and E) eruptive fissures. Refer to Fig. 4 for fissure (A), (C), (D) and (E) locations. Grey lines correspond to offset values on the western border and black lines to values on the eastern border of each fissure. 5(c) Estimation of the offset (parallel and perpendicular components) of the 1991 eruptive fissure (B). Refer to Fig. 4 for fissure (B) location. Although its signature is clear in the data, the 1991 eruptive fissure opening could not be accurately measured probably because the deformation is spread across several small fissures rather than localized, generating a noisy deformation pattern in that area. Moreover, lava flows in 1991 covers much of the fracture, yielding low ρ.

(Fig. 5a). For that, we measured the offset field on both edges of selected eruptive fissures in areas where lava flows did not cover the surface, yielding $\rho > 0.4$ (Figs 5b and c). The results are plotted in Fig. 5 as an offset versus geo-location graph. We observe that each fissure widens in a non-uniform fashion and each side shows different amounts of deformation. Moreover, fissures open and deform the ground with two components, parallel and orthogonal to their direction. Although widening is non-uniform along each fissure, we can state that there is an average opening of about 1 m with a maximum widening of 1.8 ± 0.42 m occurring on fracture 1992b. Correlation around the 1991 main fissure is poor, which is due to significant surface changes. In particular, the 1991 fissure partially overlaps the 1990 lava flow. Moreover, deformation around the 1991 fissure is spread across several small fractures rather than localized, generating a noisy deformation pattern in that area. Therefore, measurements around the 1991 eruptive fissure are less dense or missing.

6 MAPPING LAVA FLOWS

An interesting side-result of this study is shown in Fig. 6. This figure illustrates that it is possible to use the correlation-score image to map surface changes due to lava flows resurfacing between the two image acquisitions. This map has been produced by choosing pixels with $\rho < 0.3$ and supervising the results with *a priori* knowledge about the 1990, 1991, 1992 lava flow locations (Toutain *et al.* 1990, 1991, 1992a). We think that this methodology could be run automatically if images are acquired routinely before and after a single particular eruption. The correlation-score image in Fig. 6(a) has also been useful to double-check the location of each eruptive fissure. A comparison between Figs 6(b) and 2 shows a good fit between the ground-based map and the coherence-based map.

7 DISCUSSION AND CONCLUSIONS

We measured ground deformation between 1989 and 1997 on Piton de la Fournaise volcano by correlating two panchromatic airborne images. During the study period, no SAR data were available on Piton de la Fournaise. The offset results clearly show broad flank deformation of the east–southeast side of the summit area. The deformation is the result of several inflation/deflation eruptive cycles and consequent emplacement of dyke intrusions in 1990, 1991 and 1992. Offsets between the 1989 and 1997 images represent cumulative displacement of the summit area and correspond to the sum of several stages of Piton de la Fournaise activity.

Fissure geometry on Piton de la Fournaise is typically *en echelon*, which exhibits splays of fractures rather than a single one. We found that the flank deformation is not only due to new fissures opening (eruptions in 1990, 1991 and 1992) but also to reactivation of pre-existing fractures. This observation is supported by the overlap between changes in offset gradient and part of the non-eruptive fracture pattern. Pre-existing fractures have been possibly reactivated by either an inflation–deflation cycle in the 1989–1997 period, gravitational sliding between 1989 and 1997 or sporadic movements due to ground shaking crises during dyke intrusions. Development of arrays of strainmeters monitoring the opening of fractures on Piton de la Fournaise would help in discriminating among the aforementioned hypotheses in the future. We notice that reactivated fractures largely outline the unstable sector ESE of Dolomieu crater. By measuring offsets around the main eruptive fissures we found that the way each fissure widens is non-uniform along its length. The fact that offsets measured by correlation are comparatively consistent with displacement vectors acquired in a slightly different period using geodetic data acquired in the field corroborates our results. Still, we can observe a general underestimation of deformation retrieved by correlation offset in respect to ground geodetic data. This might be due to the different monitoring time period and probably to underestimation of long wavelength offset bias. Moreover, offset measures are averaged on a 21.7 m correlation window (31×31 pixels) while geodetic data correspond to point wise measures, which partially explains the misfit at GPS location.

The B/H ratio between the images, even though small, is not zero. Therefore, we expect orthorectification residual to bias the offset measurement. Further low frequency bias might come from temporary and permanent thermo mechanical deformation of negative films. Film distortions could yield low frequency bias with magnitude greater than 1 m and thus putting severe limitation in the accuracy of the offset measures at long wavelength (Michel &

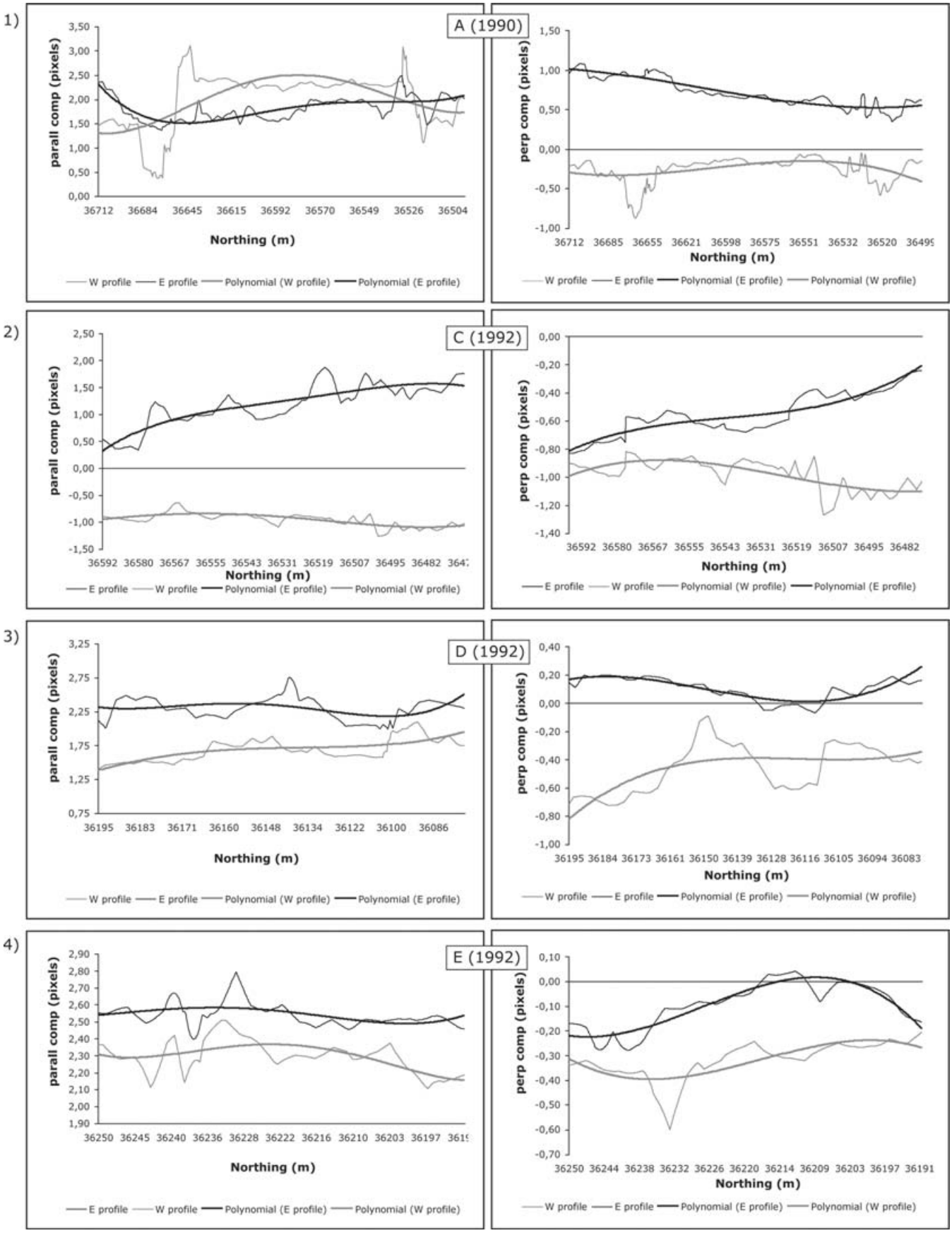

Figure 5. (b) (*Continued*.)

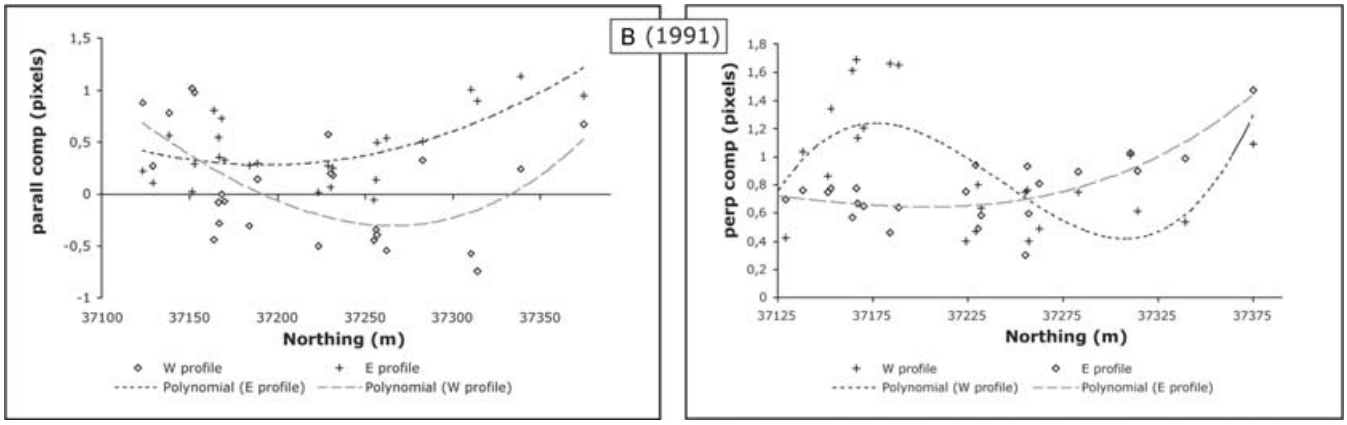

Figure 5. (c) (*Continued*.)

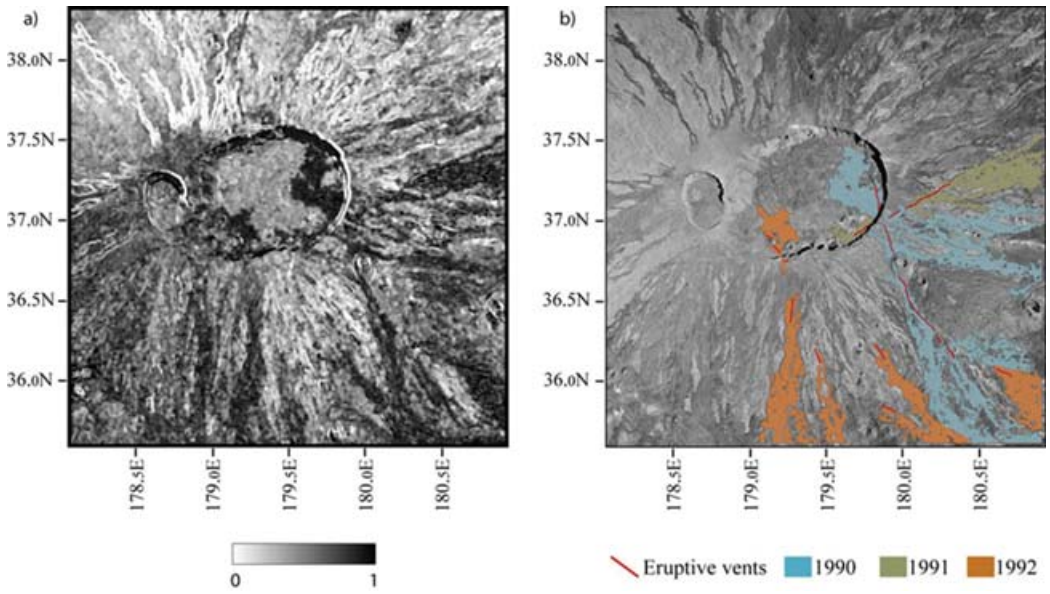

Figure 6. Correlation coefficient image yields scores in terms of radiometric changes between the orthoimages. New lava flows being one of the most significant source of radiometric change, a map of the 1990, 1991 and 1992 lava flows could be inferred from the correlation coefficient image in (a). Pixels with correlation index lower than 0.3 and *a posteriori* knowledge have been used to estimate the location of new lava flows and produce the map in (b). See Fig. 2 for comparison.

Avouac 2006). This could also partially explain the misfits between the ground geodetic measurements and offset at GPS locations in the present study. Nonetheless, low frequency residuals do not prevent the accurate measurement of fracture opening as a relative movement across eruptive fractures.

A possible improvement of the measurement method used in this study would be the independent estimation of the uncorrelated bias amplitude still present in the displacement map. This estimation would be feasible by correlating ortho-rectified air-photos acquired on the summit area over a period in which no deformation has occurred. Unfortunately, our archive does not contain data suitable for such analysis.

An ideal data acquisition configuration would consist of air-photos acquired routinely with virtually zero baseline ($B/H = 0$). In this way, (1) there would be a large number of data available, (2) the data would not be biased by temporal decorrelation due to differences in solar illumination or changes in the ground surface and (3) there would be virtually zero uncertainty due to DEM inaccuracies.

Eight years have passed between the first and the second photo acquisition. Differences in solar illumination and changes of the volcano surface (like new lava flows and ancient lava flows erosion) contributed to decorrelation. We performed a decorrelation analysis to map new lava flows, since new lava flows generate one of the most important sources of decorrelation in this study. Lava flow mapping transcends the aims of this paper, so it is not discussed deeply. Nevertheless, we illustrate the potential of this technique for remote lava flow mapping.

In conclusion, eruptions of 1990, 1991 and 1992 on Piton de la Fournaise volcano produced an important summit deformation, which could be mapped by correlation of panchromatic airborne images. Fracture patterns between 1989 and 1997 outline an unstable area in the ESE fraction of Dolomieu crater. Monitoring in terms of both deformation and lava flow mapping could be improved by routinely acquiring data from the same point of view. Correlograms derived from panchromatic imagery have shown the potential for volcanic deformation measurements as a complement to differential SAR interferometry and GPS displacement measurement.

ACKNOWLEDGMENTS

This study has been carried out in the frame of the Space Volcanoes Observatory (SVO) project (Briole, 1998) supported by CNES. We wish to thank Hélène Vadon (CNES) and Remi Michel (CEA) for fruitful discussions. We are grateful to two anonymous reviewers whose comments and suggestions improved our manuscript.

REFERENCES

Binet, R. & Bollinger, R., 2005. Horizontal coseismic deformation of the Bam (Iran) earthquake measured from SPOT-5 THR satellite imagery, *Geophys. Res. Lett.,* **32,** L02307.

Berthier, E., Vadon, H., Baratoux, D., Arnaud, Y., Vincent, C., Feigk, K.L., Rémi, F. & Legrésy, B., 2005. Surface motion of mountain glaciers derived from satellite optical imagery, *Remote Sens. Environ.,* **95,** 14–28.

Briole, P., 1998. SVO (Space Volcanoes Observatory) a proposal in response to ESA AO for Earth Explorer Opportunity Mission, http://pcsgen4.ipgp.jussieu.fr/pb/pro_esa99_svo9.pdf, 2005.

Briole, P., Bachelery, P., Mc Guire, B., Moss, J., Ruegg, J.C. & Sabourault, P., 1998. Deformation of Piton de la Fournaise: evolution of the monitoring techniques and knowledge acquired in the last five years, *The European laboratory volcanoes, Proceedings of the second workshop Santorini, Greece 2 to 4 May 1996*, 467–474.

Centre National d'Etude Spatiales (CNES), 2000. Manuel Utilisateur MEDICIS.

Crippen, R.E., 1992. Measurements of sub resolution terrain displacements using Spot panchromatic imagery, *Episodes,* **15,** 56–61.

Delacourt, C., Allemand, P., Casson, B. & Vadon, H., 2004. Velocity field of 'La Clapiere' landslide measured by correlation of aerial and Quickbird satellite images, *Geophys. Res. Lett.,* **31,** L15619.

Dominguez, S., Avouac, J.P. & Michel, R., 2003. Horizontal coseismic deformation of the 1999 Chi-Chi earthquake measured from SPOT satellite images: implications for the seismic cycle along the western foothills of central Taiwan, *J. geophys. Res.,* **108**(B2), doi:10.1029/2001JB000951.

Fialko, Y., Sandwell, D., SImons, M. & Rosen, P., 2005. Three dimensional deformation caused bu the Bam, Iran, earthquake and the origin of shallow slip deficit, *Nature,* **435/19,** 295–299.

Froger, J-L., Fukushima,, Y., Briole, P., Staudacher, T., Suriot, T. & Villeneuve, N., 2004. The deformation field of the August 2003 eruption at Piton de la Fournaise, Reunion Island, mapped by ASAR interferometry, *Geophys. Res. Lett.,* **31,** L14601.

Fukushima, Y., Cayol, V. & Durand P., 2005. Finding realistic dike models from interferometric synthetic aperture radar data: The February 2000 eruption at Piton de la Fournaise, *J. geophys. Res.,* **110**(B0), 03206, doi: 10.1029/2004JB003268.

Lenat, J.F., Malengreau, B.G. & Galdeano, A., 2001. A new model for the evolution of the volcanic island of Reunion (Indian Ocean), *J. geophys. Res.,* **106**(B5), 8645–8663.

Kninger, Y., Michel, R. & King, G.C.P., 2006. Evidences for an earthquake barrier model from $M_w \sim 7.8$ Kokoxili (Tibet) earthquake slip distribution, *Earth planet. Sci. Lett.,* **242,** 354–364.

Merle, O. & Lenat, J.F., 2003. Hybrid collapse mechanism at Piton de La Fournaise volcano, Reunion Island, Indian Ocean, *J. geophys. Res.,* **108**(B3), 2166, doi: 10.1029/2002JB002014.

Michel, R. & Avouac, J.P., 1999. Measuring ground displacement from SAR amplitude images: application to the Landers earthquake, *Geophys. Res. Lett.,* **26,** 875–878.

Michel, R. & Avouac, J.P., 2002. Deformation due to the 17 August 1999 Izmit, Turkey, earthquake measured from SPOT images, *J. geophys. Res.,* **107**(B4), 2062, doi: 10.1029/2000JB000102.

Michel, R. & Avouac, J.P., 2006. Coseismic surface deformation from air photos: The Kickapoo step over in the 1992 Landers rupture, *J. geophys. Res.,* **111,** B03408, doi: 10.1029/2005JB003776.

Nercessian, A., Hirn, A., Lepine, J.C. & Sapin, M., 1995. Internal structure of Piton de la Fournaise volcano from seismic wave propagation and earthquake distribution, *J. Volc. Geotherm. Res.,* **70,** 123–143.

Sigmundsson, F., Durand, P.D. & Massonnet, D., 1999. Opening of an eruptive fissure and seaward displacement at Piton de la Fournaise volcano measured by RADARSAT satellite radar interferometry, *Geophys. Res. Lett.,* **26,** 533–536.

Tobita, M., Murakami, M., Nakagava, H., Yarai, H. & Rosen, P.A., 2001. 3-D surface deformation of the 2000 Usu eruption measured by matching of SAR images, *Geophys. Res. Lett.,* **28,** 4291–4294.

Toutain, J.P. *et al.,* 1990. Piton de la Fournaise, *Bull. Glob. Volcan. Netw. Smiths. Inst.,* **15,** 02.

Toutain, J.P. *et al.,* 1991. Piton de la Fournaise, *Bull. Glob. Volcan. Netw. Smiths. Inst.,* **16,** 07.

Toutain, J.P. *et al.,* 1992a. Piton de la Fournaise, *Bull. Glob. Volcan. Netw. Smiths. Inst.,* **17,** 09.

Toutain, J.P., Bachelery, P., Blum, P.A., Cheminee, J.L., Delorme, H., Fontaine, L., Kowlawsky, P. & Taochy, P., 1992b. Real time monitoring of vertical ground deformation during eruptions at Piton de la Fournaise, *Geophys. Res. Lett.,* **20,** 553–556.

Trembley, I. & Briole, P., 2005. The 5 meters grid size Digital Elevation Model (DEM) of Piton de la Fournaise summit area; improving resolution and accuracy by image correlation technique and kinematic GPS, *IPGP Internal Report*, http://geodesie.ipgp.jussieu.fr, 2005.

Van Puymbroeck, N., Michel, R., Binet, R., Avouac, J.P. & Taboury, J., 2000. Measuring earthquakes from optical satellite images, *Appl. Opt.,* **39,** 3486–3494.